

Bearing Currents and Their Relationship to PWM Drives

Doyle Busse, Jay Erdman, *Member, IEEE*, Russel J. Kerkman, *Senior Member, IEEE*,
Dave Schlegel, *Member, IEEE*, and Gary Skibinski, *Member, IEEE*

Abstract—This paper examines ac motor shaft voltages and the resulting bearing currents when operated under pulse width modulation (PWM) voltage source inverters. The paper reviews the mechanical and electrical characteristics of the bearings and motor in relation to shaft voltages and bearing currents. A brief review of previous work is addressed, including the system model and experimental results. The theory of electric discharge machining (EDM) is presented, including component calculations of the system elements. The effect of system elements on shaft voltages and bearing currents are evaluated experimentally and the results compared to theory. A design calculation is proposed that provides the relative potential for EDM. Finally, the paper will present quantitative results on one solution to the shaft voltage and bearing current problem.

Index Terms—Bearing capacitance, bearing current, bearing current density, bearing threshold voltage, electric discharge machining, electrostatic shielded induction motor, rotor shaft to ground voltage, stator to rotor capacitance.

I. INTRODUCTION

IN RECENT YEARS, the powering of induction motors from variable frequency drives (VFD) has become increasingly popular. Even though the induction motor is a very rugged device, the bearings are now subject to additional modes of failure due to bearing currents. Bearing currents in larger ac motors have been known for many years. The cause has been understood to be induced by magnetic dissymmetries in the construction of the motor resulting in destructive bearing currents.

Shaft voltages and their resulting currents were recognized by Alger [1] in the 1920's. Since then, numerous investigations of the problem have been reported with recent contributions by Costello and Lawson [2], [3]. In recent years, the effect of pulse width modulation (PWM) drives operating ac motors has been studied. All motors have some level of shaft voltage and resulting bearing current. In addition, bipolar junction transistor (BJT) and insulated gate bipolar transistor (IGBT) inverters experience electric discharge machining (EDM) currents. Two key elements are which voltage conditions will break down the insulating grease film and how the resulting current densities affect bearing life.

This paper will focus on the mechanisms that cause these voltages and the ability of bearings to withstand the resulting currents. Possible mechanisms for bearing damage when

operating on VFD include electric field breakdown of the oil film resulting in EDM currents and lower level dv/dt or electrostatically induced currents altering the chemical composition of the lubricant.

Recently, the authors presented their findings on EDM and its relationship to PWM inverter operation [4]. In contrast to traditional magnetic imbalance effects found in sine wave-driven machines, it was shown that PWM inverters serve to excite a capacitive coupling between the stator and rotor. This coupling combined with the high-frequency electrical characteristics of the bearing allow the motor shaft voltage to instantaneously achieve potentials over 20 times that observed on sine wave operation.

The current resulting from the motor shaft voltage is limited by the bearing impedance. As motor speed increases, the bearing resistance attains values in the megohm range [4]. Technical literature indicates that as speed increases, the balls ride an oil film, forming a boundary between the race and the ball with the exception of instantaneous asperity point contacts. An asperity is the deviation from the mean surface, usually in microns.

Fig. 1 shows the surface roughness of a bearing race that demonstrates electrical fluting damage [5]. The paper investigates the theoretical and empirical basis of bearing oil film charging with PWM voltage source inverters. The dielectric strength of typical lubricating films is determined along with an explanation of why the film can withstand rotor shaft voltages in the range of 10 to 30 V peak for short periods.

This paper explores the relevant bearing failure mechanisms in addition to the failure indicators of shaft voltage and bearing current magnitudes. The point contact area is calculated and a current density is specified to project bearing life. The paper presents motor and bearing capacitance characteristics for a wide horsepower range and relates them to an equivalent common mode motor and bearing model. A steady-state analysis of the full model leads to the development of a voltage ratio, which is convenient for analyzing the potential for shaft voltages and bearing currents. A reduced second-order model is proposed for analysis purposes. Experimental results, examined in the context of the second-order model, demonstrate the effects of drive system components on shaft voltages, and how the excitation voltage, coupling capacitances, and bearing characteristics relate to EDM and dv/dt currents. Finally, the paper will analyze a proposed solution to the bearing current problem and quantify the improvement by comparing the magnitudes of dv/dt and EDM currents.

Manuscript received January 24, 1996; revised July 26, 1996.

The authors are with Rockwell Automation—Allen Bradley Company, Mequon, WI 53092 USA.

Publisher Item Identifier S 0885-8993(97)01959-5.

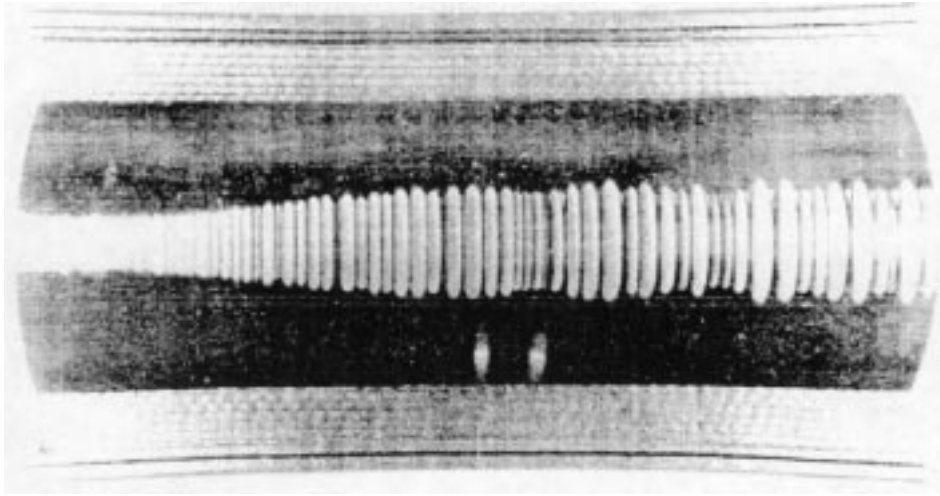


Fig. 1. Surface roughness of a ball bearing race [5].

II. SAFE BEARING CURRENT LEVELS

This section of the paper will describe electrostatically induced bearing failure mechanisms. It discusses shaft voltages as a failure indicator and proposes current magnitudes as an additional indicator for PWM voltage source inverters. A theory of Hertzian contact area is provided and employed to calculate the bearing current density and bearing life degradation.

A. Failure Mechanisms of Bearings

Bearing failures can be attributed to induced bearing currents in addition to traditional mechanical and thermal failure mechanisms. Bearing currents can result from machine construction or the type of application. Mechanical failures can be produced by excessive vibration, while thermal failures result from overloads, which increase bearing temperature and decrease mechanical life. Perhaps the most common mechanical failure is subsurface cracking, due to normal contact stresses, resulting in spalling or flaking of the race surface. A surprisingly large number of failures are due to improper installation.

Machines contain magnetic dissymmetries inducing end to end rotor shaft voltage that result in bearing current. Bearing current and its induced mechanical wear do not exist if shaft voltage is less than a critical bearing threshold voltage ($V_{th}(\Delta)$) required to break down the insulating grease, which is a function of lubricant thickness and surface roughness (Δ) [6]. $V_{th}(\Delta)$ is 0.2 to 1 V under 60-Hz sine wave operation [7], [8]. Low bearing currents result when shaft voltage is slightly greater than $V_{th}(\Delta)$ and induce a chemical change of low resistivity lubricants, ultimately reducing life by raceway corrosion [9]. High shaft voltages, resulting from the bearing oil film acting as a capacitor in high-resistivity lubricants, which is charged to common mode voltage levels, may produce damaging EDM currents. When race to ball asperity contacts come close, the oil film's electric field increases, leading to breakdown with high discharge currents that create a localized elevated temperature of the race and results in molten pits. The pits eventually lead to fluting of Fig. 1 and reduced mechanical life [10]. Small machines typically maintain a shaft voltage less

than $V_{th}(\Delta)$ threshold. Large machines may employ lubricants with increased $V_{th}(\Delta)$, thus reducing EDM current [11].

Machine applications with belt-driven rotors or in ionized air are known to exhibit electrostatically induced charge on the bearing capacitance (C_b) and possibly result in damaging EDM current. PWM motor drives are known to naturally charge C_b thru the stator to rotor coupling capacitance (C_{sr}). Rotor to ground voltage (V_{rg}) is determined by voltage divider action between C_{sr} , the parallel combination of rotor to frame capacitance (C_{rf}) and C_b , and stator neutral to ground voltage (V_{sng}) of Fig. 2. Since V_{sng} modulates around 0 V with peaks of plus and minus 1/2 bus voltage (V_{bus}), the rotor shaft voltage charges to high open circuit voltages, before asperity contact closure causes film breakdown. With high V_{sng} values, PWM inverters produce higher EDM currents than those observed with sine wave operation. Furthermore, V_{sng} induces dv/dt currents through the bearing film and also through bearing asperity points when in contact. The common mode equivalent model of Fig. 2 will be used throughout this paper, with all the components explained. More detailed analyzes and parameter measurement techniques for the model may be found in [4], [12], and [13].

B. Shaft Voltage as a Degradation Indicator

End to end *axial shaft voltages* >200 mVrms on sine wave excitation indicate magnetic dissymmetry, creating high localized bearing current. The magnitude of the *rotor shaft voltage to ground* is an indication that excessive wear may occur when operated on PWM driven drives. Fig. 3 shows three different shaft voltage phenomenon occurring in a bearing lubricated with high resistivity grease.

Region A (115–265 μ S): V_{sng} and C_{sr} charge the high-resistivity mineral oil film forming C_b . A plateau value, determined by C_{sr} in series with $(C_b || C_{rf})$ capacitive divider action, is explained in Section III. At the end of *Region A*, V_{sng} modulates to a higher level, causing the V_{rg} to increase. The oil film breaks down at 35 Vpk, creating a 3-Apk EDM pulse. Film thickness is typically 0.2 to 2 μ m depending on oil temperature [8]. Lower film thickness occurs at higher bearing

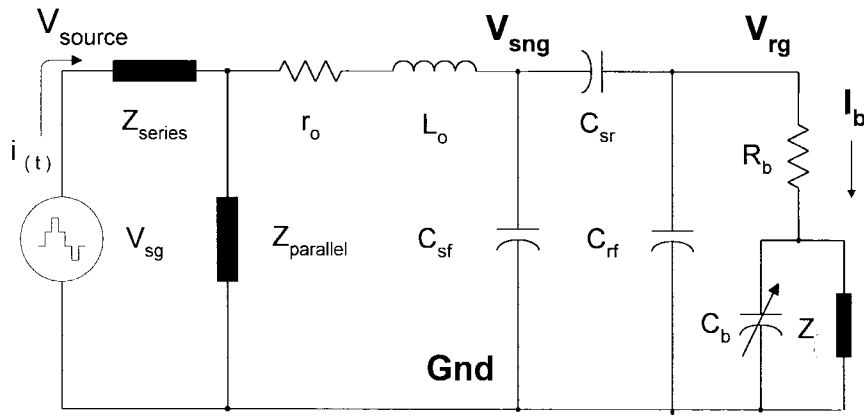


Fig. 2. Common mode equivalent model.

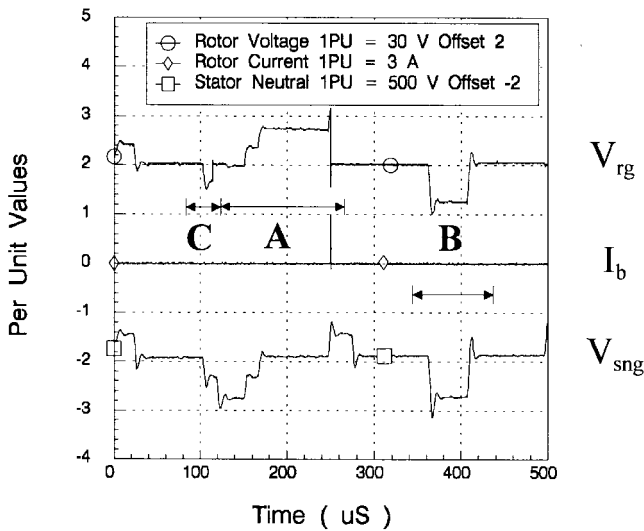


Fig. 3. Examples of bearing breakdown mechanisms due to film breakdown, dv/dt currents, and asperity contacts.

temperature. The breakdown for a 2- μm film @ 25 °C with 400-V/mil mineral oil at typical PWM frequencies is 30 Vpk. However, breakdown values decrease to 6–10 V as the motor heats up, agreeing with film thickness theory.

Region B (340–440 μs): V_{sng} and C_{sr} charge C_b by capacitive divider action. The plateau value is less than the 30-Vpk breakdown value, therefore no EDM occurs. V_{rg} is replicated by divider action as V_{sng} returns to zero. The power device switching time determines dv/dt current levels. Peak dv/dt currents of IGBT drives are 200–500 mA while BJT drives have 50 mA or less.

Region C (80–115 μs): V_{sng} and C_{sr} charge C_b by capacitive divider action but to a lower value than the 35 Vpk of *Region A*. Even before V_{sng} modulates upward, the 10-Vpk plateau value instantaneously breaks down, indicating EDM discharge. Here, rolling asperity contacts reduce the film thickness at the point contact, resulting in a $V_{\text{th}}(\Delta)$ lower than $V_{\text{th}}(\Delta)$ of the oil film thickness of *Region A*.

Regions of V_{rg} at 0 V with V_{sng} at high levels are explained by asperity contacts shorting out C_b to a low resistance. Inner and outer race random contact duration of asperity contacts is 33 and 100 μs at low speed and 12 and 40 μs at high

speed, respectively. Bearing dv/dt currents of 100–500-mA peak also occur when asperities short C_b while V_{sng} switches.

C. Current Magnitude as an Indicator of Bearing Degradation

Establishing a maximum allowable bearing current magnitude is difficult without knowing surface contact area of the passing current and grease composition. A nonrotating bearing may pass large sine wave currents without damage because larger contact area occurs [8]. Also, bearing current magnitude failure mechanisms are sensitive to the type of grease. High-resistivity mineral oil greases act as capacitors with high $V_{\text{th}}(\Delta)$, which produce EDM currents and arcing on discharge. This failure is best analyzed using bearing current density. High-resistivity greases with low bearing currents do not produce arcing, but may produce fritting. Fritting tempers the steel, which lowers surface hardness and allows accelerated mechanical wear. Low-resistivity lithium grease does not exhibit a $V_{\text{th}}(\Delta)$, but acts as a resistor. Currents of 189-mA rms (267-mA peak) cause grease decomposition into lithium iron oxide, leading to increased wear and bearing failure [9]. Values of 0.5-A rms accelerate corrosion and fritting [9]. Thus, EDM currents and dv/dt currents should be analyzed for allowable bearing current density and peak currents <267 mApk for corrosive effects and fritting.

D. Bearing Contact Area

In a stationary bearing or bearing rotating at low speed, there is a larger contact area between race and ball, mainly consisting of quasimetallic surfaces that puncture through the oil film. Increased bearing contact area (mm^2) implies larger bearing current magnitudes (A) are required to cause temperatures high enough to melt and pit the race. Applications of rotating bearings with no shaft load, where the rotor weight alone would divide equally over one to three balls provide the smallest contact areas. Thus, bearing current density (A/mm^2) is a preferred indicator of bearing life under pitting and fluting.

Accurate calculation of actual contact surface area in a rotating bearing is difficult, since it depends on surface roughness, “asperity contacts,” and on the oil film thickness, which itself is a function of grease viscosity, grease temperature, motor speed, and motor load. Fig. 4 shows an equivalent

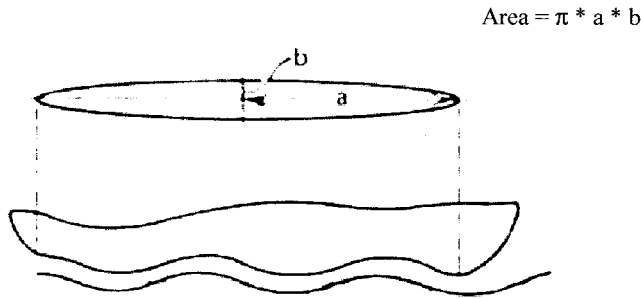


Fig. 4. Hertzian ellipse used to calculate the asperity contact area.

Hertzian ellipse area under a surface roughness and waviness of associated asperity contacts. The Hertzian ellipse point contact area (mm^2) is calculated using a sequence of equations to determine the major (a) and minor (b) foci and multiplying them by π . The sequence of equations as provided by Harris [14], with a complete summary of the Hertzian ellipse contact area provided in [12].

E. Bearing Current Density Versus Life Degradation

Bearing current density has been proposed on sine wave-driven machines to predict bearing life under the influence of current passing through the bearing. Haus [15] determined 0.7 A/mm^2 for 50 000 h bearing life, while 1.4 A/mm^2 shortened life to 500 h. Krumpolc [16] determined 0.1 A/mm^2 as totally safe. Kulda [17] quotes 1.0 A/mm^2 as tolerable, 1.4 A/mm^2 as a destruction level after 500 h, and values $>2 \text{ A/mm}^2$ causing destruction after 5 h. Endo [18] quotes 1.0 A/mm^2 as a critical density value while from field experience 1.8 A/mm^2 caused failure in 2 h and values $<0.15 \text{ A/mm}^2$ up to 0.39 A/mm^2 are time proven safe values with no signs of fluting.

Bearing current testing is historically based on ac line operation, (60-Hz nominal sinewave measured in Arms), with a bearing rotating at rated base speed and using high-resistivity grease. Bearing life is therefore based on destructive currents occurring in high-resistivity grease. The authors translated the current density data, using the above referenced literature, into the graph of Fig. 5. By converting historical current density limits of (Amp rms/ mm^2) to (Amp peak/ mm^2) bearing life is estimated with EDM and dv/dt bearing currents under PWM operation. However, more research on pulsed EDM life is required. Equation (1) describes electrical bearing life in Fig. 5. Additional current density information is provided in [12]:

$$\text{Electrical Bearing Life [hr]} = 7867204 * 10^{-\left(2.17\left(\frac{A_{pk}}{\text{mm}^2}\right)\right)} \quad (1)$$

It is the authors' best estimate for the effects of pulsed voltage waveforms on bearings. Speed, load, and grease temperature establish the mechanical life of a bearing [19]. This life is derated by nonmechanical factors. The L_{10} life establishes a lower limit for bearing life and for industrial applications is typically 20 000–40 000 h [10], with useful mechanical life approaching 40 000–60 000 h. A more complete explanation of mechanical life is provided in [12]. Finally, the authors propose the maximum bearing current density with PWM

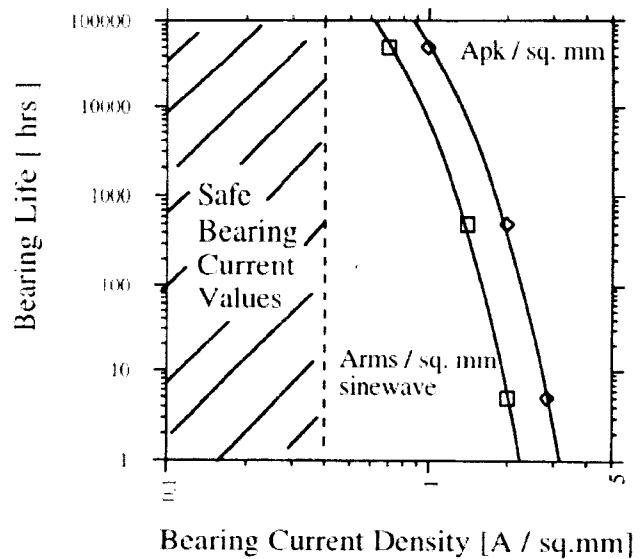


Fig. 5. 60-Hertz ac line bearing current density versus life curve.

drives to be $<0.8 \text{ (Apk/mm}^2\text{)}$ to insure bearing current does not limit the mechanical life of the bearing.

III. EFFECT OF DRIVE SYSTEM VARIABLES ON ELECTROSTATIC BEARING CURRENT

In accompanying papers [4], [12], [13], the authors presented a drive system model for the purpose of analyzing shaft voltages and bearing currents present with PWM voltage source inverters. The inverter was modeled as a balanced three phase source with a common mode or zero sequence source from neutral to ground. The motor consisted of two sets of balanced three phase windings coupled by an equivalent π network of machine capacitances. The bearing model consisted of a bearing resistance (R_b) in series with a parallel combination of bearing capacitance (C_b) and a nonlinear device (Z_l). The nonlinear device accounts for the charging and discharging of the shaft.

For purposes of shaft voltage buildup, dv/dt current, and EDM discharge investigations, a common mode or zero sequence equivalent circuit is preferred. Fig. 2 represents the zero sequence equivalent circuit of the system model in [4]. Included in this circuit are the common mode effects of the ac machine, long cable lengths, common mode chokes and transformers, and line reactors. The model contains the source impedance elements (Z_{series} and Z_{parallel}), the motor equivalent impedances (the stator winding zero sequence impedance (L_o and R_o), the stator winding to frame capacitance (C_{sf} , C_{sr} , and C_{rf}), and the bearing model (R_b , C_b , and Z_l).

From Fig. 2, it is clear the existence of EDM currents with PWM voltage source inverter drives depends on the following three conditions: 1) a source of excitation, which is provided by the source voltage to ground (V_{sg}); 2) a capacitive coupling mechanism, accomplished by C_{sr} ; and 3) sufficient rotor voltage buildup, a random occurrence depending on the existence of C_b . All three of these conditions must simultaneously exist for EDM to occur.

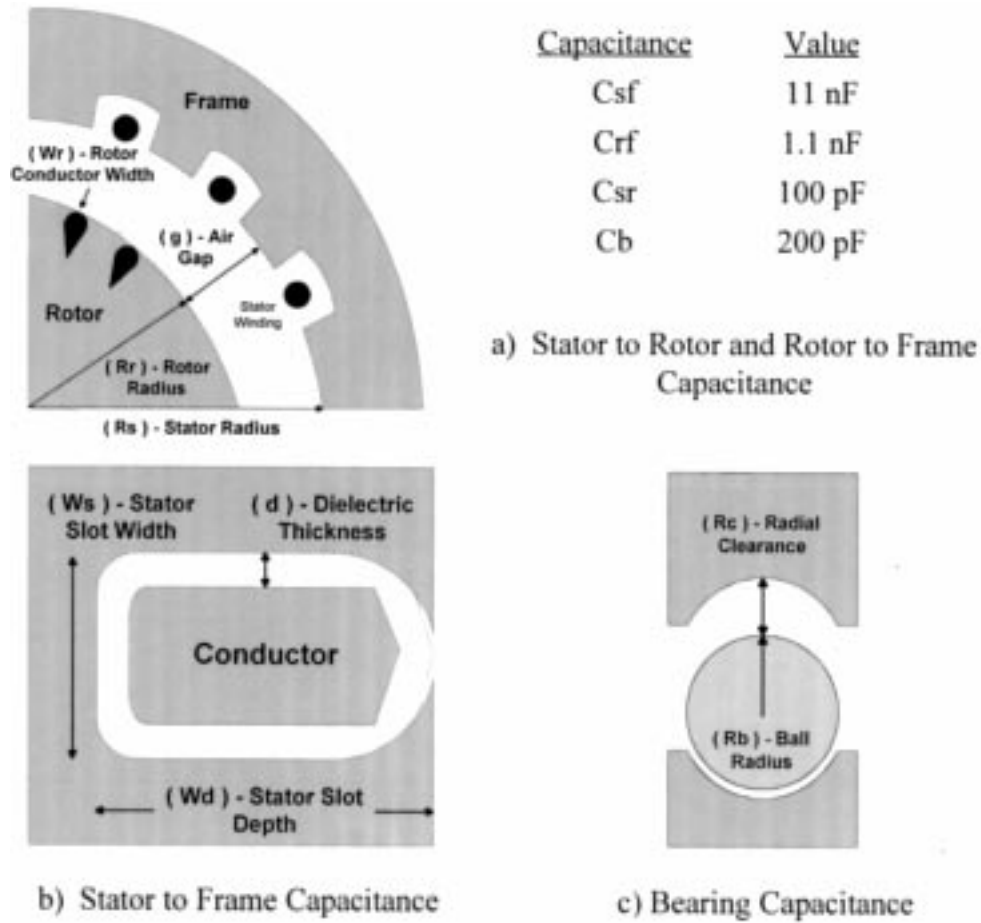


Fig. 6. Capacitance model physical descriptions: (a) stator to rotor and rotor to frame capacitance; (b) stator to frame capacitance; (c) bearing capacitance.

This section of the paper will explore the contributing system factors to the development of shaft voltage buildup. Part A will present relevant mechanical properties and results from induction machine capacitance calculations for the system components of Fig. 2. Experimental evaluations of system capacitances for the 15 hp machine of [4] are included.

Part B of this section examines drive variables—common mode chokes, line reactors, long cables—and their effect on shaft voltage and bearing current. The common mode circuit above is reduced in complexity and a simple analysis tool is presented. Finally, a design equation—the Bearing Voltage Ratio (BVR)—establishes a machine design criteria for evaluating the potential for shaft voltages and bearing currents.

A. Effect of Motor Variables on Electrostatic Bearing Current

Mechanical Variables: The potential for shaft voltages and bearing currents depends on the existence of C_b . Furthermore, the bearing impedance becomes capacitive only when a lubricant film occurs in the contact regions between the balls or rollers and the raceways. The minimum film thickness is given by

$$H^0 = 2.65\bar{U}^{0.7}g^{0.54}/\bar{Q}_z^{0.13} \quad (2)$$

where U is a function of the fluid velocity and viscosity, g is a function of the pressure coefficient of viscosity and modulus of elasticity, and Q is the force or load acting on the ball or roller [14]. The bearing capacitance, therefore, is a function of radial load, velocity, temperature (T), lubricant dielectric strength (ϵ_r), and viscosity (λ)—($C_b(Q, U, T, \epsilon_r, \lambda)$).

Electrical Variables—System Impedance: The system impedance of Fig. 2 is composed of L_o , R_o , C_{sf} , C_{sr} , C_{rf} , and C_b . Although they are distributed in nature, a lumped parameter representation is employed in modeling the system.

L_o and R_o : The common mode or zero sequence impedance of the machine equals one third of the stator resistance in series with one third of the stator leakage inductance; it was obtained by connecting all three lines together and measuring line-to-neutral with a Hewlett-Packard 4284A LCR meter. A value of 300 μ H and 59.8 Ω was measured at 100 kHz.

System Capacitances: This section will present the results of capacitance calculations for a wide range in horsepower assuming geometrical shapes of a standard induction motor and a typical ball bearing and compare them to experimental values for the 15-hp machine of [4]. Fig. 6 depicts each of the relevant capacitances: (a) C_{sr} and C_{rf} ; (b) C_{sf} ; (c) C_b . Fig. 7 shows the calculated values for each capacitance as a function of horsepower for machines from 5–900 hp [20]–[22]. These calculations were based on design data for four pole, 460-Vac induction machines and associated bearing dimensions.

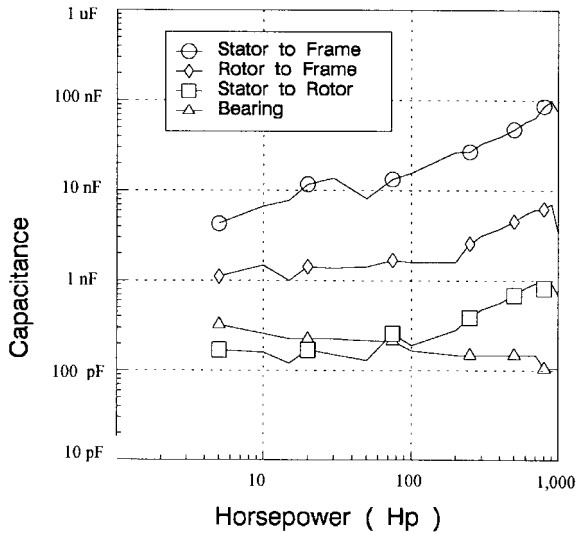


Fig. 7. Motor and bearing capacitance calculation values.

Actual capacitance values for the machine of [4] are listed in the Fig. 6 for comparison purposes.

B. Effect of Drive Variables on Electrostatic Bearing Current

System Model and Analysis: With the common mode model for the drive established, an analysis of the effects of system parameters on shaft voltages and bearing currents is possible. Fig. 2 allows for the investigation of common mode chokes or transformers, line reactors, and long cables through the modification of the series and parallel impedance elements (Z_{series} and $Z_{parallel}$); it provides the capability to examine PWM modulation techniques and power device rise times, and it allows for an investigation of voltage levels.

Steady-State Shaft Voltage Level: With PWM frequencies much less than the natural frequency of the zero sequence system impedance, the capacitances divide V_{sng} and yield the following algebraic relationship for the BVR:

$$BVR = V_{rg}/V_{sng} = C_{sr}/(C_{sr} + C_b + C_{rf}), \quad (3)$$

This relationship, although simple, provides substantial information about bearing charge and discharge phenomena and potential improvements. For example, $V_{th}(\Delta)$ exists for each value of film thickness below which dielectric breakdown EDM does not occur. This threshold depends on pulse duration and characteristics of the lubricant. For example, with a dielectric strength or electric field intensity of 15 Vpk/ μm and lubricant film thickness varying between 0.2 and 2 μm , the $V_{th}(\Delta)$ varies from 3 to 30 Vpk.

Equation (3) also suggests a large C_b reduces V_{rg} ; thus, to maintain the bearing voltage below $V_{th}(\Delta)$ —the maximum sustainable voltage without dielectric breakdown EDM—increase the relative permittivity of the lubricant. This expression also shows how an electrostatically shielded induction motor (ESIM) eliminates the potential for shaft/bearing static voltage buildup— C_{sr} in (3) is zero for an ESIM. In addition, the capacitive voltage divider indicates inserting an insulating sleeve or barrier may exacerbate the bearing charging since this reduces the effective C_b .

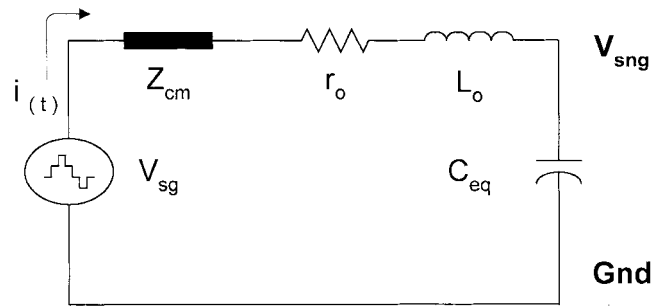


Fig. 8. Reduced-order common mode model.

Fig. 3 shows a typical sequence of V_{sng} , bearing current (I_b), and V_{rg} traces for the 15-hp motor of [4]. The BVR is obtained by dividing the shaft voltage by V_{sng} at a point where the machine's rotor rides the lubricant, region A for example. The experimental value—0.064—is in good agreement with the theoretical calculations of 0.074.

Second-Order Model Approximation: The common mode model of Fig. 2 adequately describes most of the observed phenomena associated with shaft voltages and common mode currents. However, the complexity of this model often obscures the cause and effect on shaft/bearing voltages and currents observed with PWM voltage source inverters. A reduced-order model, if applied correctly, would have a distinct advantage to the circuit of Fig. 2. For example, common mode chokes, line reactors, and output filters often are employed to reduce electromagnetic interference from PWM voltage source inverters. Also, many applications require long cable lengths between the inverter and load. The reduced-order model of Fig. 8 allows for an easy evaluation of the effects of these elements on V_{sng} of the machine [20], [22].

The second order system of Fig. 8 has the following general solution for a step input:

$$V_{sng} = V_{sg} \left(1 - \frac{1}{\sqrt{1-\zeta^2}} e^{-\zeta\omega_n t} \sin(\omega_n \sqrt{1-\zeta^2} t + \psi) \right) \quad (4)$$

$$i(t) = \frac{V_{sg}}{\sqrt{1-\zeta^2} Z_o} e^{-\zeta\omega_n t} \sin \omega_n \sqrt{1-\zeta^2} t. \quad (5)$$

where

$$\omega_n = \frac{1}{\sqrt{L_o C_{eq}}}, \quad \zeta = \frac{r_o}{2} \sqrt{\frac{C_{eq}}{L_o}},$$

$$Z_o = \sqrt{\frac{L_o}{C_{eq}}}, \quad \psi = A \tan \left(\frac{\sqrt{1-\zeta^2}}{\zeta} \right)$$

and ω_n is the undamped natural frequency, ζ is the damping ratio, and Z_o is the characteristic impedance. The equivalent capacitance (C_{eq}) equals $C_{sf}/((C_{sr} + C_{rf})/C_b)$ —the stator to frame capacitance in parallel with the series combination of the stator to rotor capacitance and the parallel combination of the rotor to frame and bearing capacitances.

This formulation of the system equations also allows for an easy analysis of the rise time of V_{sg} , the effect of the PWM frequency, and influence of system parameters on damping, natural frequency, and overshoot. If the rise time of the stepped

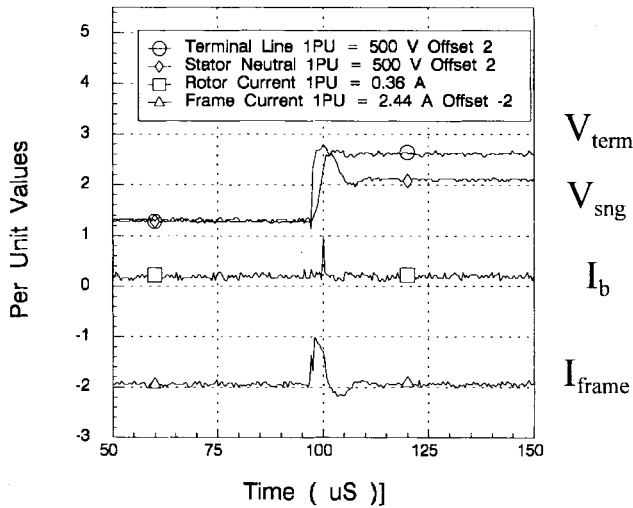


Fig. 9. IGBT voltage step experimental results.

line to neutral voltage is longer than one half of the oscillation period, the zero sequence current is reduced substantially, thus reducing the dv/dt current through the bearing and frame. Furthermore, increasing the common mode inductance—with common mode chokes and line reactors—without considering the effect on the damping factor can raise the Q of the circuit. The higher Q and lower natural frequency may result in a near resonance with the stepped waveform of the forcing function's PWM carrier.

Evaluation of Reduced-Order Model: Fig. 9 shows typical experimental results of tests performed on an IGBT PWM voltage source inverter with an induction motor load. The leading trace shows the machine terminal voltage (V_{term}) to ground and the following trace V_{sng} voltage. The terminal voltage appears as a step function to the machine and the neutral voltage responds as a RLC load. V_{sng} oscillates at 100 kHz with a damping ratio of 0.21. Using the reduced order model and the C_{eq} , L_o , and R_o for the 15-hp machine, the calculated values are 84.3 kHz and 0.26, respectively. In [4], the authors show good correlation between the experimental and simulation results using the full motor model. By utilizing the reduced model, incorporating the BVR of (3) and the voltage and current frequency response equations of (4) and (5), reasonably accurate results are obtainable. Estimates of V_{sng} and V_{rg} are possible using a spreadsheet analysis without time consuming simulations. Therefore, Fig. 8 provides a simple design and analysis tool for evaluating the common mode voltage source and its effects on shaft/bearing voltage buildup.

Effects of Common Mode Components, Line Reactors, and Cable Lengths: With the advent of IGBT inverter drives, common mode noise presents a significant challenge to drive design. Common mode chokes and transformers inserted between the inverter output and the load motor provide additional impedance to common mode current without affecting the fundamental component. Another approach inserts a three-phase line reactor, but at the price of reduced fundamental voltage at the terminals of the machine.

Fig. 10 shows the response of V_{sng} , and V_{rg} , and I_b with a common mode choke of 270 μH and 2.6 Ω inserted between

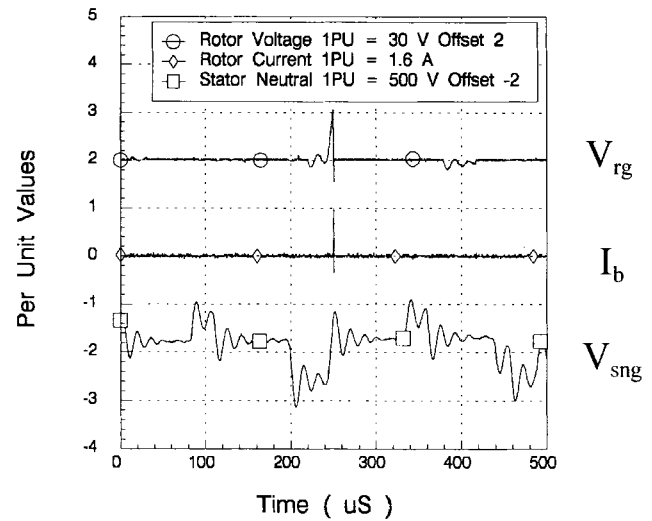


Fig. 10. Common mode choke experimental results.

the inverter output and load motor. The neutral to ground voltage oscillates at 60 kHz with a damping ratio of 0.12. Using the model of Fig. 8, the calculated values are 62.7 kHz and a damping factor of 0.12.

Adding the common mode choke to reduce dv/dt current also affects the response of V_{sng} and V_{rg} . The reduced damping causes the machine's neutral voltage to overshoot the steady-state value for each switching instant. The decreased damping also provides the rotor the opportunity to charge once the bearing rides the lubricant film.

To examine the effects of reduced damping in more detail, a three-phase series reactor with a common mode reactance of 600 μH was inserted between the inverter output and load motor. The calculated frequency of oscillation and damping factor for the system were 50.3 kHz and 0.0158, respectively.

Experimental results for the 15-hp machine (Fig. 11) show a lightly damped 50-kHz oscillation. The decrease in damping increases the probability of C_b charging. Because the system capacitance never achieves the steady-state charge associated with the forcing function, each time the bearing rides the film, the system topology changes and the voltage distribution changes in response to the impedance change. Finally, V_{sng} exceeds 590 Vpk, which is 280 Vpk larger than $V_{bus}/2$.

Cable length has an important effect on the dv/dt current, and an equally important effect on shaft voltage buildup and bearing current discharge. Fig. 12 shows V_{sng} , V_{rg} , and bearing current with a 600-ft cable. At the frequencies of interest, the cable presented an equivalent series impedance of 3.2 Ω and 80 μH , and a parallel resistance of 3.0 Ω in series with 22 nF of capacitance. The Thévenin equivalent equals a resistance of 10.9 Ω in series with 129 μH . The calculated damped natural frequency and damping ratio for Fig. 8 are 71.7 kHz and 0.18. These compare well with the experimental values of 76.0 kHz and 0.19.

The transient response of the long cable system shows V_{sng} rings up to over 600 Vpk, with a nominal 630-Vdc bus. The bearing rides the lubricant film and charges to 25 Vpk just prior to the ring up of V_{sng} . Once the stator begins to ring up to the 600-Vpk level, V_{rg} responds with a slight delay

TABLE I
CALCULATED BEARING LIFE WITH PWM IGBT DRIVES AND 15-hp MOTOR

Parameter	Units	Standard AC Motor		ESIM Motor	
		Rotor Weight	3 Times Rotor Weight	Rotor Weight	3 Times Rotor Weight
EDM Current	Apk	2.2	2.2	0	0
Contact Area	mm ²	0.62	1.29	0.62	1.29
Current Density	Apk/mm ²	3.5	1.7	0	0
Calculated Life	hrs	< 10	1,570	> 100,000	> 100,000
dv/dt Current	Apk	0.2 - 0.5	0.2 - 0.5	0.05	0.05
Contact Area	mm ²	0.62	1.29	0.62	1.29
Current Density	Apk/mm ²	0.32 - 0.8	0.15 - 0.38	0.08	0.04
Calculated Life	hrs	> 100,000	> 100,000	> 100,000	> 100,000

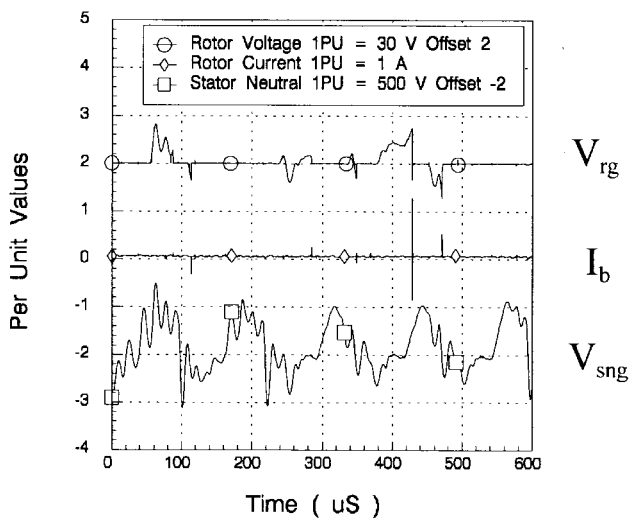


Fig. 11. Common mode reactor experimental results.

and achieves almost 65-Vpk peak before an EDM of 3.2 Apk occurs. Experimental results similar to these confirm excessive neutral and shaft voltages are possible with long cable lengths. The resulting current densities—5.16 to 2.48 Apk/mm²—are in the region to reduce bearing life.

Effects of Bus Voltage, Pulse Duration, and Modulation Techniques: Experiments were performed on the 15-hp drive at various bus voltage levels, carrier frequencies, and modulation techniques. The results showed shaft voltages and bearing currents were present for all voltage levels—230-Vac, 460-Vac, and 575-Vac drives—and modulation strategies. Pulse duration, however, does determine the occurrence of one form of EDM—lubricant breakdown discharge.

As discussed in [4], the dielectric strength or electric field intensity of a material depends on duration of the voltage pulse applied. An investigation into the voltage threshold for EDM showed with a 275 V_{bus} and pulse duration of 100 mS, EDM's were essentially eliminated. This corresponds to a rotor voltage of 10 Vpk. Raising V_{bus} such that the rotor voltage increased to 18 Vpk and comparing the EDM currents for 2- and 8-kHz carrier frequencies showed 2-kHz operation with eight times the EDM discharges. Thus, for typical lubricants, the dielectric strength as a function of pulse duration has a similar

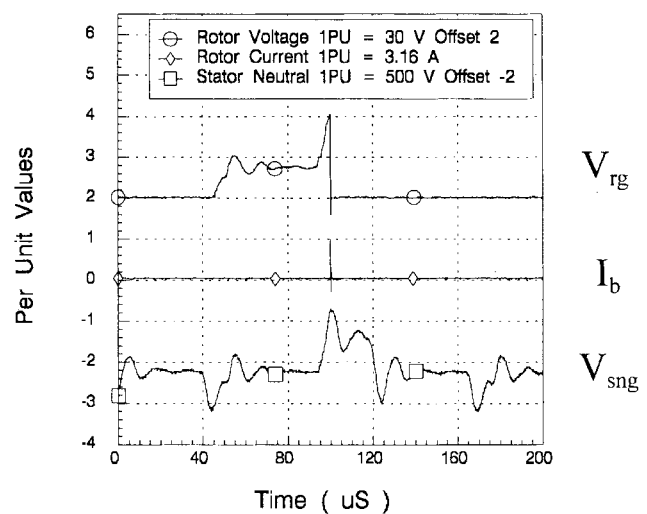


Fig. 12. Long cable length experimental results.

relationship to that of hexane [4]. The electric field intensity (E_{th}) is a function of the PWM pulse duration and lubricant, while $V_{th}(\Lambda)$, the associated scalar potential, is a function of the lubricant thickness and surface roughness (Λ).

IV. BEARING LIFE PROJECTION WITH AN ESIM

Bearing contact area was calculated for applications with no shaft load (rotor weight alone) and with three times rotor weight. Bearing current density uses measured peak EDM and dv/dt currents and calculated contact area. Estimated bearing life is found from Fig. 5 or (1). The process was repeated with EDM and dv/dt currents measured with the electrostatic shielded induction motor (ESIM) [4].

Table I shows that dv/dt currents do not accelerate bearing degradation and reduce bearing life. Unloaded motors are more susceptible to EDM bearing damage than loaded motors. Calculated bearing life must be tempered by realizing the difficulty of determining contact area and that worst case contact area with one ball was assumed. Force may be distributed over one to three ball bearings, increasing contact area, while distributing EDM current pulses. How Fig. 5 (60-Hz ac line bearing current density versus life curve) correlates to life with PWM pulsed EDM currents remains unknown. However,

EDM bearing current densities less than 0.6 to 0.8 Apk/mm² probably do not degrade bearing life. Accurate life predictions are difficult due to the steepness of the life curve, e.g., from 0.8 to 2.0 Apk/mm² life is greatly decreased.

Table I shows the ESIM proposed in [4], [12], [13], and [23] appears promising as a solution to bearing current problems, since destructive EDM pulse currents are eliminated and dv/dt current is reduced to <50 mApk. Since dv/dt current is <267 mApk limit for low level current corrosion and fritting, this problem is also eliminated. Thus, loaded or unloaded, bearing life approaching 100 000 h is now attainable with mechanical limitations determining ultimate life.

V. CONCLUSION

The paper presented a review of the mechanisms that cause bearing currents. Theoretical calculation and measurement verification of the equivalent circuit impedances of the electrical model were presented. Shaft voltages and the resulting bearing currents were measured and their components identified. With typical lubricant dielectric strengths, rotor voltages in excess of 30 Vpk were measured.

The theory of bearing contact area calculation was presented and a current density versus life projection was made. Lubrication plays an important role in this issue. Further work needs to be done to show the effects of different lubrication materials affecting bearing currents. A search of the literature indicates that currents of 0.2 to 0.5 Arms/mm² on a sine wave basis will result in a reasonable useful life. The author's propose the maximum bearing current density with PWM drives to be <0.8 (Apk/mm²) to insure bearing current does not limit the mechanical life of the bearing.

Experimental results with PWM voltage source inverters and typical system components demonstrated possible rotor voltages far in excess of the nominal 30 Vpk. The EDM currents produced current densities of over 5.0 Apk/mm².

The data indicates that an ESIM is capable of reducing bearing currents to a level that exhibits reasonable life. The resulting dv/dt and EDM currents produce current densities in line with those observed on sine wave operation.

ACKNOWLEDGMENT

The authors wish to thank D. Conrad of Dodge-Reliance, L. Cox of Bearings, Inc., S. Evon of Reliance Electric, D. Hyypio of Marathon Electric, G. Lynk of Torrington Bearing, J. Misch of NTN Bearing, and J. Tevaarwerk of Emerson Electric for their assistance in this research project. The motor was provided by Marathon Electric.

REFERENCES

- [1] P. Alger and H. Samson, "Shaft currents in electric machines," in *A.I.R.E. Conf.*, Feb. 1924, pp. 235-245.
- [2] M. Costello, "Shaft voltage and rotating machinery," *IEEE Trans. Ind. Applicat.*, vol. 29, pp. 419-425, Mar. 1993.
- [3] J. Lawson, "Motor bearing fluting," CH3331-6/93/0000-0032 1993-IEEE.
- [4] J. Erdman, R. J. Kerkman, D. Schlegel, and G. Skibinski, "Effect of PWM inverters on AC motor bearing currents and shaft voltages," *IEEE Trans. Ind. Applicat.*, vol. 32, pp. 250-259, Mar./Apr. 1996.

- [5] T. Tallian, G. Baile, H. Dalal, and O. Gustafsson, "Rolling bearing damage—A morphological atlas," SKF Industries, Inc., Technology Center, King of Prussia, PA.
- [6] H. Kaufman and J. Boyd, "The conduction of current in bearings," in *ASLE Conf.*, 1958.
- [7] NEMA MG-1 Specification Part 31, Section IV, 1993.
- [8] S. Andreason, "Passage of electrical current thru rolling bearings," SKF Gothenburg.
- [9] S. Murray and P. Lewis, "Effect of electrical currents on ball bearing damage in vacuum and air," in *22nd ASLE Annu. Meet.*, May 1, 1967.
- [10] J. L. Tevaarwerk and W. A. Glaeser, "Tribology," University of Wisconsin-Milwaukee, College of Engineering & Applied Science, Center for Continuing Engineering Education, May 15-16, 1995.
- [11] S. Komatsuzaki, T. Uematsu, and F. Nakano, "Bearing damage by electrical wear and its effect on deterioration of lubricating grease," *ASLE*, vol. 43, no. 1, pp. 25-30, 1987.
- [12] D. Busse, J. Erdman, R. J. Kerkman, D. Schlegel, and G. Skibinski, "The effects of PWM voltage source inverters on the mechanical performance of rolling bearings," in *IEEE Applied Power Electronics Conf.*, Mar. 3-7, 1996, pp. 561-569.
- [13] ———, "System electrical parameters and their effects on bearing currents," in *IEEE Applied Power Electronics Conf.*, Mar. 3-7, 1996, pp. 570-578.
- [14] T. Harris, *Rolling Bearing Analysis*, 3rd ed. New York: Wiley, 1991.
- [15] O. Haus, "Shaft voltage and bearing currents—Causes, effects and remedies," *ETZ-A*, pp. 105-112, 1964.
- [16] E. Krumpolc, "Bearing currents and shaft voltages in electric machines," *Electrotechnik*, vol. 45, no. 4, pp. 88-91, Apr. 1990.
- [17] V. Kulda, "Bearing currents in electrical machines," *The Electrical Engineer*, vol. 20, no. 11, pp. 323-326, 1965.
- [18] H. Endo, *Analysis of Current Density at D.C. Motor Bearing*, Shinko Electric Ltd., Jan. 21, 1978.
- [19] A. Bonnett, "Cause and analysis of anti-friction bearing failures in AC induction motors," US Electrical Motors, Inc., St. Louis, MO.
- [20] H. W. Hayt, *Engineering Electromagnetics*, 5th ed. New York: McGraw-Hill, 1989.
- [21] H. Prashad, "Theoretical evaluation of capacitance, capacitive reactance, resistance and their effects on performance of hydrodynamic journal bearings," *Trans. ASME*, vol. 113, pp. 762-767, Oct. 1991.
- [22] J. L. Melsa and D. G. Schultz, *Linear Control Systems*. New York: McGraw-Hill, 1969.
- [23] D. Busse, J. Erdman, R. J. Kerkman, D. Schlegel, and G. Skibinski, "An evaluation of the electrostatic shielded induction motor: A solution for rotor shaft voltage buildup and bearing currents," in *Ind. Applicat. Society Conf. Rec.*, San Diego, CA, 1996, pp. 610-617.



Doyle Busse received the A.A.S. degree in electrical engineering technology from the Waukesha County Technical College, Waukesha, WI, in 1986. He continued his education at the Milwaukee School of Engineering, where he received the B.S. degree in electrical engineering in 1989.

He has been with the Rockwell Automation-Allen Bradley Company, Mequon, WI, since 1990, where he is currently a Senior Test Engineer.



Jay Erdman (M'58) received the B.S.E.E. degree from the Milwaukee School of Engineering, Milwaukee, WI, in 1958.

He recently retired from the Rockwell Automation-Allen Bradley Company, Mequon, WI, where he was employed since 1958. He was most recently an Industry Consultant, where he specialized in the application of adjustable frequency drives and motors.

Mr. Erdman is a member of TAPPI (Technical Association of the Pulp and Paper Industry).



Russel Kerkman (S'67-M'76-SM'88) received the B.S.E.E., M.S.E.E., and Ph.D. degrees in electrical engineering from Purdue University, West Lafayette, IN, in 1971, 1973, and 1976, respectively.

From 1976 to 1980, he was an Electrical Engineer in the Power Electronics Laboratory of Corporate Research and Development, General Electric Company, Schenectady, NY. He is currently a Senior Principal Engineer for the Rockwell Automation-Allen Bradley Company, Mequon, WI. His current interests include: the modeling and

control of general purpose industrial drives, adaptive control applied field oriented induction machines, the application of observers to ac machines, and EMI from PWM inverters.



Dave Schlegel (M'90) received the A.A.S. and B.S.E.E.T. degrees in electrical power engineering technology from the Milwaukee School of Engineering, Milwaukee, WI, in 1990 and 1996, respectively.

He has been with the Rockwell Automation-Allen Bradley Company, Mequon, WI, since 1979, where he is currently a Development Engineer.

Mr. Schlegel is a member of STLE (Society of Tribologists and Lubrication Engineers).



Gary L. Skibinski (M'74) received the B.S.E.E. and M.S.E.E. degrees from the University of Wisconsin, Milwaukee, and the Ph.D. degree from the University of Wisconsin, Madison, in 1976, 1980, and 1992, respectively.

From 1976 to 1980, he was an Electrical Engineer working on Naval Nuclear Power at Eaton Corporation. From 1981 to 1985, he worked on servo controllers at the Allen Bradley Company as a Senior Project Engineer. During the Ph.D. program, he was a Consultant for UPS and switchmode power supply products at the R.T.E. Corporation.

Dr. Skibinski is currently a Principal Engineer at the Rockwell Automation-Allen Bradley Company, Mequon, WI. His current interests include: power semiconductors, power electronic applications, and high-frequency high-power converter circuits for ac drives.